

Effects of Magnetic Conducting Boundary on Design of Electromagnetic Actuators Using Image method

Hungsun Son¹, Kok-Meng Lee², Jun Yeob Song³, Jongkweon Park⁴

^{1,3,4}Intelligent Manufacturing Systems Research Division, Korea Institute of Machinery and Materials, South Korea

¹(Tel:82-42-868-7362; E-mail: hson@kimm.re.kr)

³(Tel:82-42-868-7144; E-mail: sjy658@kimm.re.kr) ⁴(Tel:82-42-868-7116; E-mail: jkpark@kimm.re.kr)

²Woodruff School of Mechanical Engineering, Georgia Institute of Technology, Atlanta, GA, U.S.A
(Tel : 1-404-894-3204; E-mail: kokmeng.lee@me.gatech.edu)

Abstract: Design and control of multi degrees of freedom (DOF) electromagnetic actuators often require understanding the magnetic fields of a permanent magnet (PM), an electromagnet (EM) and a magnetic material boundary. This paper presents an image method to characterize the magnetic field of a permanent magnet (PM), magnetic conducting boundary, and its use in computing the magnetic torque of PM-based actuators. In particular, the method offers an effective means to optimize design parameters that could significantly affect the torque and force performance of a multi-DOF electromagnetic actuator. While developed in the context of the multi-DOF actuator, the modeling techniques presented in this paper are applicable to design of other PM-based actuators.

Keywords: Permanent magnet, magnetic field, image method, magnetic conducting boundary, torque model, spherical motor

1. INTRODUCTION

The demand for increasing accuracy, high speed and flexibility of micro-machines can be found in numerous applications such as manufacturing, precision machining [1] and micro-factory [2]. Most of the applications require orientation control of a tool and a workpiece. Recently, the growing interests in fuel-cell technology and low-cost electromechanical systems have motivated a number of researchers to develop compact and high efficient multi-DOF electromagnetic actuators. In the design and analysis of such novel electromechanical actuators, both accurate and fast computations of magnetic field distributions and force/torque models are often required.

Existing techniques for analyzing electromagnetic fields and designing multi-DOF PM-based actuators primarily rely on three approaches; namely, analytic solutions to Laplace's equation, numerical methods [3] and lumped-parameter analyses with some form of magnetic equivalent circuits (MEC) [4]. However, these existing approaches have difficulties in achieving both accuracy and low computation time simultaneously. In addition, many engineering problems with PMs or EMs are often required to solve the three dimensional (3D) magnetic field with/without a magnetic conducting interface. These difficulties have led us to develop a new modeling method to derive closed-form field solutions for efficient design and accurate motion control of the actuators. In [5], distributed multi-pole (DMP) model has been developed using magnetic pole models. The DMP modeling method can be used to characterize the magnetic field distribution in open space. Since the DMP method is here based on the concept of magnetic dipole and a limited set of known field information to construct a distributed dipole model, the method offers a relatively complete formulation for deriving the closed-form and an effective means to characterize the magnetic fields and torque

computations for design and control of electromagnetic actuators. However, the method mainly focused on characterizing the magnetic field of a PM (or an EM) in free space. When the magnetic field is involving a magnetic conducting material, the field of the PM or EM interacts with the material boundary. In addition, the change of the field distribution results in the consequent change of the magnetic force and torque. To account for the effects of the material boundary on the DMP method, an image method can be applied along with the DMP modeling method.

The image method is commonly used for analyzing boundary problems of electromagnetic fields since the method provides certain solution forms for some important problems involving straight-line, circular and spherical boundaries in a simple manner which decrease the need for formal solutions of Laplace's and Poisson's equations. The image method in [6] is used to analyze the unbounded magnetic field containing ferromagnetic materials by a numerical method (FEM). The magnetic field in two dimensional space to design a electromagnetic actuator are obtained in analytical forms using image and MEC methods [7]. Unlike the solutions in [7] with the first order accuracy, nonlinear approach is used to account for effects of eddy currents with magnetic conducting boundary [8]. However, the methods in [8] is mainly applicable for a simple structure of a conductive rod in a simplified geometry.

In this paper, we extend the DMP method to handle the magnetic conducting boundary using an image method. The methods developed here offer a relatively complete solution of the magnetic field involving magnetic conducting boundaries and thus, the methods can be used to design an electromagnetic actuator.

The remainder of this paper offers the following:

1. We review and formulate general boundary conditions of material interfaces in magnetic field using magnetic surface charges.

2. We formulate relatively closed-form solutions of magnetic fields using the image method to account for magnetic boundary interference. Then, two different boundaries are illustrated in the three dimensional (3D) space; plane and sphere. In particular, we derived the solutions in non-dimensional forms in order to investigate the effects of the boundary interface to magnetic field distributions. Once magnetic poles from the DMP method and the image method are found, the magnetic field can be efficiently computed and applied to design electromagnetic actuators.
3. We demonstrate an image method with the DMP modeling using two examples, which illustrate the procedure of the image method. In the examples, the simulated results of the DMP and image methods are also validated to compare the numerical method using ANSYS. In addition, the effectiveness of the methods will be also shown by comparing the computational time.

2. ANALYSIS METHOD

The principle of an image method replaces the effects of a boundary or material interface on an applied field by adding or subtracting elementary fields behind the boundary line called image charge. Provided image charges for the magnetic material boundary, the resultant field distribution with the material boundary can be expressed as the sum of the applied and the image fields. Two boundary conditions; normal and tangential directions of the interface between two regions can be summarized as follows:

Condition I: Normal component of \mathbf{B} is continuous across the boundary

$$\mathbf{B}_1 \cdot \mathbf{n} = \mathbf{B}_2 \cdot \mathbf{n} \quad (1)$$

Condition II: Tangential component of \mathbf{H} is continuous along the boundary

$$(\mathbf{H}_1 - \mathbf{H}_2) \times \mathbf{n} = 0 \quad (2)$$

where subscripts 1 and 2 denote the regions between the boundary respectively

Based on the image method to compute the magnetic field with a boundary, each region of the boundary on the given field requires different images but one side of images leads to the other. Since the field distribution for two regions are connected by the boundary conditions (1) and (2), the solutions in each region can be achieved at once.

Figure 1 shows an arbitrary shape of a boundary in the magnetic field. A region 1 with permeability μ_1 is separated from a region 2 with permeability μ_2 by the boundary with a local coordinate system.

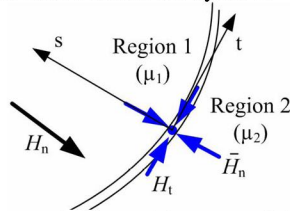


Fig. 1 Magnetic flux with a material boundary

Supposed that H_n is the normal component of the existing magnetic field in the region 1. If the different material with permeability μ_2 is presented in the original region with μ_1 , the magnetic flux is discontinuous at the boundary due to the magnetic surface charge. The effect of the surface charge at the boundary can be accounted for by a normal component of field \bar{H}_n and considered to act in the same direction as H_n in the region 1 and the opposite direction in the region 2 (blue arrow in Fig. 1). The resultant normal field at a point on the boundary becomes $H_n + \bar{H}_n$ in region 1 and $H_n - \bar{H}_n$ in region 2. Thus, the net field strength of the entire space with the region 1 with the source and 2 without the source remain the same as the open space with the source in the region 1.

Since the normal component of flux is continuous across the boundary in (1), it is necessary to satisfy

$$\mu_1 (H_n + \bar{H}_n) = \mu_2 (H_n - \bar{H}_n) \quad (3)$$

Thus, the net normal component of the field H_{1n} at the interface of the region 1 is given by

$$H_{1n} = \left(\frac{2\mu_2}{\mu_2 + \mu_1} \right) H_n \quad (4)$$

Similarly, H_{2n} at the interface of the region 2 is given by

$$H_{2n} = \left(\frac{2\mu_1}{\mu_2 + \mu_1} \right) H_n \quad (5)$$

From (4) and (5), the net normal component of the field intensity at the interface of regions 1 and 2 can be expressed in non-dimensional forms by

$$\frac{H_{1n}}{H_n} \Big|_{s=0} = \frac{2}{1+\rho} \quad \text{and} \quad \frac{H_{2n}}{H_n} \Big|_{s=0} = \frac{2\rho}{1+\rho}$$

where $\rho = \mu_1 / \mu_2$; s denote the coordinate system shown in Fig. 1.

Similar to the normal component in (4) and (5), the tangential component of the magnetic field from (2) at the boundary can also be obtained as follows:

$$H_{1t} + \bar{H}_t = H_{2t} + \bar{H}_t \quad (6)$$

Once the field \mathbf{H} along the boundary is found, the scalar potential function can be inversely computed from \mathbf{H} . Since the field in the region of interest should not include image charges, the general expression of the potential can be given by

$$\Phi_i = \Phi_u - \bar{\Phi}_i \quad (7)$$

where the subscript i denotes the region of interest (normally $i=1, 2$ between the boundary); the subscript u denotes the solution without the boundary.

In particular, the scalar potential in (7) can be assumed as a constant if the boundary is the magnetic conducting material which the permeability μ in the boundary is large. This characteristic can be shown as an illustrative example in the next section where spherical magnetic-conducting boundary in the three dimension space will be presented. In addition, the example shows the design procedures of spherical actuators using DMP and image method.

Plane Boundary

To illustrate the image method, we simplify the DMP method and consider here a single source with a plane boundary shown in Fig. 2. The plane boundary provides the fundamental understanding of the image method and thus the results of this can be also extended to solve more complicated shape of boundaries by various combinations and conformal transformation. In addition, the DMP method satisfies superposition principle for the solution of Laplacian field, the single source model can be extended to the DMP model without loss of generality.

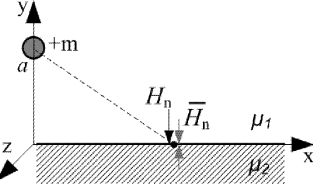


Fig. 2 Source with plane boundary

The net normal and tangent components of \mathbf{H} at the interface of the regions 1 and 2 due to the source at the boundary point $P(x, 0, z)$ in Fig. 2 are given by:

$$H_n(x, y, z) = \frac{\mp |m|(Y-1)}{4\pi a^2} \left[X^2 + (Y-1)^2 + Z^2 \right]^{-3/2} \quad (8)$$

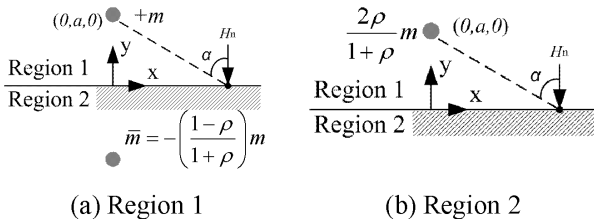
$$H_t(x, y, z) = \frac{\mp |m|X}{4\pi a^2} \left[X^2 + (Y-1)^2 + Z^2 \right]^{-3/2} \quad (9)$$

where $X = x/a$; $Y = y/a$; and $Z = z/a$. Due to the effect of the induced surface charge at the boundary, the normal component \bar{H}_n along the boundary is given by substitution from (8) into (3). In addition, the solution of each region is uniquely determined in such a way that the strength of the original source in the region 1 does not change by the boundary and also the region 2 does not have the source. Thus, the solution of each region can be explained by an equivalent image pole (source or sink) with $\pm m[(1-\rho)/(1+\rho)]$ as shown in

Fig. 3. The corresponding scalar potential Φ for each region can be given by summing the applied and image poles from (7) as follows:

$$\frac{\Phi_i}{\Phi_u} = 1 - \frac{\bar{\Phi}(x, y + (-1)^{i+1}a, z)}{\Phi_u} \quad (10)$$

where i denotes the corresponding region ($i=1, 2$)



(a) Region 1 (b) Region 2

Fig. 3 Equivalent charge in each region

Finally, the field of each region can be summarized as follows:

$$\text{For } Y \geq 0 \quad \frac{\Phi}{\Phi_u} = 1 - \left(\frac{1-\rho}{1+\rho} \right) S \quad (11a)$$

$$\frac{H_n}{H_{n1}} = 1 - \left(\frac{1-\rho}{1+\rho} \right) \left(\frac{Y+1}{Y-1} \right) S^3 \quad (11b)$$

$$\text{where } Y \neq 1 \quad \frac{H_t}{H_{t1}} = 1 - \left(\frac{1-\rho}{1+\rho} \right) S^3 \quad (11c)$$

$$\text{For } Y < 0 \quad \frac{\Phi}{\Phi_u} = \frac{H_n}{H_{n1}} = \frac{H_t}{H_{t1}} = \frac{2\rho}{1+\rho} \quad (11d)$$

where $S = \sqrt{[X^2 + (Y-1)^2 + Z^2]} / \sqrt{[X^2 + (Y+1)^2 + Z^2]}$.

The solutions from (11a) to (11d), guarantee the two boundary conditions of (1) and (2) at $Y=0$ ($S=1$) as follows:

$$B_{n1} = \frac{2\mu_1 H_n}{1+\rho} = B_{n2} = \frac{2\mu_2 \rho H_n}{1+\rho}; \quad H_{t1} = H_{t2} = H_n \left(\frac{2\rho}{1+\rho} \right)$$

Some observations from (11a) to (11d) can be drawn:

If the boundary plane is highly magnetic-conducting such that $\rho = \mu_2 / \mu_1 \rightarrow 0$, then B_{n1} is twice greater than the original strength of B_n . In addition, the tangential component of \mathbf{H} becomes $H_{t1} = H_{t2} \rightarrow 0$. This indicates the normal component of the magnetic flux is dominant along the boundary so that the magnetic flux is perpendicular to the surface boundary.

If the boundary plane were removed, and instead an image sink was placed a distance h behind the now missing conducting plane, then a vanishing potential can be found at midway between the applied source and the image sink. Reinserting the conducting surface along this plane would make no difference as the potential already satisfies the boundary condition ($\Phi = \text{constant}$ on a conductor).

Although the applied source $+m$ induces a nonzero source distribution on the conducting boundary in order to maintain a zero potential, the potential arising from this distribution is mimicked exactly by the image sink $-m$ behind the boundary.

Spherical Boundary

Many engineering problems with PMs or EMs are often required to solve the three dimensional (3D) magnetic field including magnetic conducting interface. However, the 3D analysis is relatively difficult to solve using the previous method by which the magnetic field \mathbf{H} (or \mathbf{B}) distribution was directly obtained. One of alternatives is using the scalar potential function since the surface of high conducting boundary can be assumed to be the equal potential. Based on this, it is possible to compute the modeling parameters of image charges inversely. We consider here a spherical boundary of a magnetic conducting material since it is commonly used for a spherical actuator illustrated later. Based on the concept of the magnetic surface charge, the boundary conditions in the 3D magnetic field can be simplified using the scalar potential function which can be assumed to be the equal potential on the surface of high conducting boundary.

Without loss of generality, the surface assigned to the constant potential of the boundary can be further reduced by coordinate transformation.

$$\Phi = 0 \quad (12)$$

Consider the magnetic source inside a magnetic conduction sphere as shown in Fig. 4. Due to the symmetry of the sphere, it can be reduced to plane view in the yz plane.

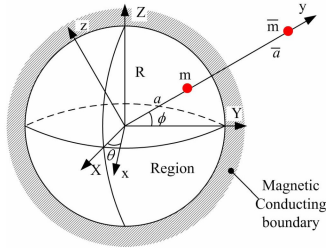


Fig. 4 Image charge of Spherical boundary

The magnetic charge with the strength m at $P(0, a \cos \phi, a \sin \phi)$ can be expressed in the xyz local frame and the potential on the spherical surface is given by

$$\Phi = -\frac{1}{4\pi} \left(\frac{m}{\sqrt{a^2 + R^2 - 2aR \cos \phi}} + \frac{\bar{m}}{\sqrt{\bar{a}^2 + R^2 - 2\bar{a}R \cos \phi}} \right) \quad (13)$$

To satisfy (12), unknown distance and strength \bar{a} , \bar{m} for the image charge in (13) can be expressed by

$$\bar{a} = R^2 / a \quad \text{or} \quad \bar{a} = a \quad (14)$$

where $\bar{a} = R^2 / a$ can be chosen since the image charge should be outside of the sphere.

Similarly, the strength of the image charge \bar{m} can be given by

$$\bar{m} = -Rm/a \quad (15)$$

Given the parameters in (14) and (15), the scalar potential function Φ inside circle can be expressed as follow:

For $0 \leq r \leq R$ region:

$$\Phi = -\frac{m}{4\pi} \left(\frac{1}{\sqrt{x^2 + (y-a)^2 + z^2}} - \frac{R/a}{\sqrt{x^2 + (y-(R^2/a))^2 + z^2}} \right) \quad (16)$$

From (16), three practical cases shown in Fig. 5 are considered here to illustrate the combination of the DMP and image method since an electromagnetic actuator generally consists of rotor, magnet and stator.

Case 1 (iron rotor): PM is outside the sphere

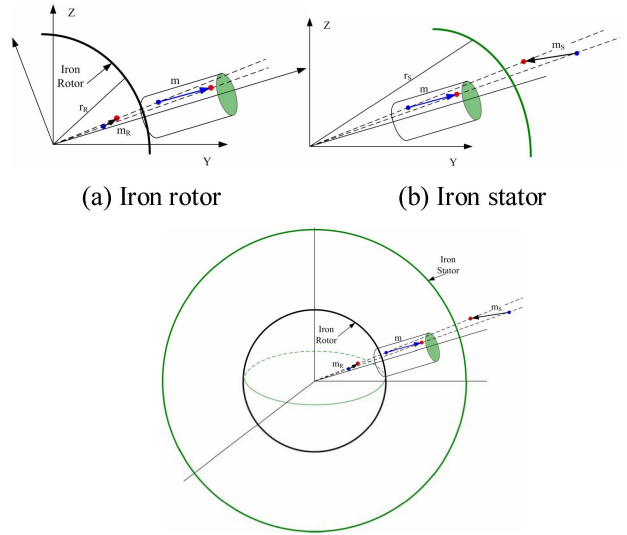
Case 2 (iron stator shell): PM is inside sphere shell

Case 3: Combination of both Case 1 and Case 2

Case 1 considers a pair of the DMP model for a permanent magnet with the strength m and rotor boundary of a radius r_R in Fig. 5(a). In (16), the position of each source/sink (x_1, y_1, z_1) can be expressed in the spherical coordinate as follows:

$$\begin{bmatrix} x_1 \\ y_1 \\ z_1 \end{bmatrix} = r_1 \begin{bmatrix} \cos \theta_1 \cos \phi_1 \\ \sin \theta_1 \cos \phi_1 \\ \sin \phi_1 \end{bmatrix} \quad (17)$$

where $r_1 = \sqrt{x^2 + y^2 + z^2}$; $\theta_1 = \tan^{-1}(y_1/x_1)$; and $\phi_1 = \cos^{-1}(z_1/r_1)$



(a) Iron rotor (b) Iron stator (c) Combination of both iron rotor and stator

Fig. 5 DMP method and image method

Since the image charge is along the line of the applied charge vector with the different distance, the position of the image charge can be expressed in terms of the ratio of lengths Λ_R from (14) and unit vector of the applied charge from (17).

$$\begin{bmatrix} \bar{x}_1 \\ \bar{y}_1 \\ \bar{z}_1 \end{bmatrix}_R = \Lambda_R r_R \begin{bmatrix} \cos \theta_1 \cos \phi_1 \\ \sin \theta_1 \cos \phi_1 \\ \sin \phi_1 \end{bmatrix} \quad (18)$$

where $\Lambda_R = r_R / r_1$; r_R is the radius of the rotor (subscript R indicates the rotor).

From (15), the strength of the image charge is also given in terms of Λ_R by

$$\bar{m}_R = -m / \Lambda_R \quad (19)$$

In Case 2, the image charge of the stator boundary with the outer radius r_S in Fig. 5(b) can be expressed in terms of the ratio $\Lambda_S = r_S / r_1$ as follows:

$$\begin{bmatrix} \bar{x}_1 \\ \bar{y}_1 \\ \bar{z}_1 \end{bmatrix}_S = \Lambda_S r_S \begin{bmatrix} \cos \theta_1 \sin \phi_1 \\ \sin \theta_1 \sin \phi_1 \\ \cos \phi_1 \end{bmatrix} \quad (20)$$

Similarly, $\bar{m}_S = -\Lambda_S m$ (21)

where the subscript S indicates the stator.

Case 3 includes both the iron rotor and stator. Since the strength and position of image charge of each case are found, Case 3 can be obtained using the principle of superposition of the solution in Cases 1 and 2.

The potential functions including each boundary can be expressed as summing each potential function of the corresponding image charges. Thus, the image method associated with the DMP model also provides the closed-form solutions about the three dimensional magnetic field with magnetic conducting boundaries.

3. ILLUSTRATIVE EXAMPLES

Two examples are simulated to validate the modeling method and also illustrate the procedure using the image method to account for the effects of magnetic boundary

conditions.

Example 1: Validation with ANSYS

Figure 6 shows the DMP with the image method and ANSYS model of a electromagnetic system with a pair of PMs and EMs. Two system configurations with and without magnetic conducting boundaries are simulated and compared against the numerical method using ANSYS.

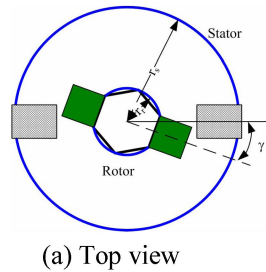
Design A: Rotor and stator are non-magnetic conductors.

Design B: Rotor and stator are magnetic conductors.

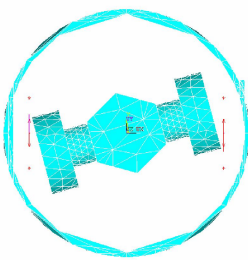
For simplicity, ANSYS model uses the cylinder iron boundary but the DMP model uses the spherical boundary. The rotor rotates at the same plane parallel to the plane of the cylinder. The simulations are based on the parameters detailed in Table 1.

Table 1 System parameters

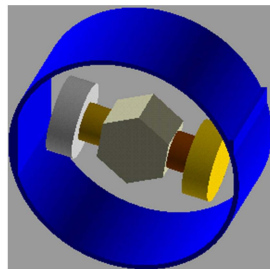
r_R	0.75 inch
r_S	2.5 inch
PM	
length	0.75 inch
Radius	0.375 inch
M_0	1.12 T
EM	
Outer radius	0.75 inch
Inner radius	0.375 inch
Length	1 inch
# of turn	1040
I	4 Amp



(a) Top view



(b) Mesh of ANSYS



(c) 3D model of ANSYS

Fig. 6 ANSYS simulation and Image method

Figure 7 shows the simulation results of the torque computation which have good agreement and the maximum errors for each configuration is less than 7% and 5% respectively. However, some discrepancies occurred from the initial position. In the FE method, the free space must be bounded due to the computational effort; particularly in 3D, the computation cost increases drastically with the size of the free space. This, along the distortion of the automatically generated FE mesh, contributes to some discrepancy (of less than 5% difference) between the two models. The mesh distortion depending on the shape of mesh could be the cause of the FE error (offset) even when the separation angle is zero.

In addition, the computational time of the results for Fig. 7 are compared. The numerical method using ANSYS took about 12 minutes to compute Design A, and 20 minutes for Design B using a Windows-based PC (dual core processor 2.21Ghz CPU and 1GB memory), while the DMP based models require less

than 17 seconds to compute each of the cases as compared in Table 2.

Table 2 Computational time (seconds)

DMP		ANSYS	
Design A	Design B	Design A	Design B
0.0128T(16)	0.013T(17)	0.5484T(702)	T=1480.

The time of the DMP-based torque calculation can be further reduced by modeling the multilayer EM as an equivalent single-layer EM or PM in [5].

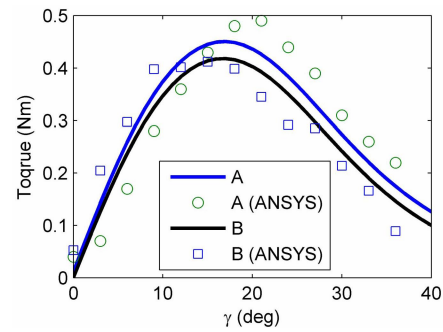


Fig. 7 Comparisons between DMP and ANSYS

Example 2: Effect of magnetic field on iron boundaries

Figure 8 shows a magnetic system which consists of two permanent magnets on the spherical rotor and one electromagnet in the stator, which is used here to investigate the effects of the iron boundaries on the magnetic field distribution and the torque.

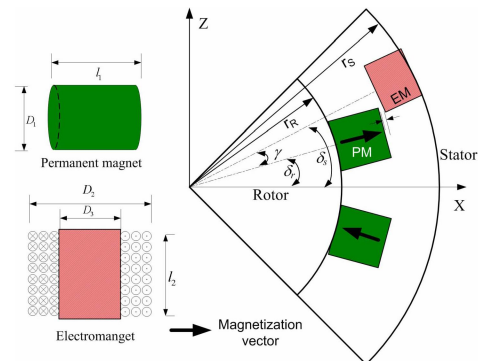


Fig. 8 Actuator with two PMs and EMs

The same parameters of the example 1 such as the size of PMs, EM, rotor and stator are used for the example 2. In addition, the computational results of the PMs for the DMP and image methods are given in Table 3. To investigate the effect of the iron boundary on the torque, four different configurations are compared:

- Case A: Rotor and stator are non-magnetic boundaries;
- Case B: Only rotor is a conducting boundary;
- Case C: Only stator is a conducting boundary;
- Case D: Rotor and stator are magnetic boundaries.

Figure 9 visualizes the magnetic field of each design. The black and red bold circles indicate the boundaries of the rotor and the stator to identify each boundary. Figure 9(a) shows the non-magnetic boundaries of rotor and stator, which serves as a basis for comparing any effect of the boundaries. Figure 9(b), (c) and (d) show

the influence of the magnetic field due to the iron rotor, iron stator and both iron rotor and stator respectively. Since current flowing through the coil conductor interacts with the magnetic field in the air-gap region, it is most critical to analyze the effects of the magnetic field on the force/torque computation. The magnetic field of Case B makes smaller change than Case C in the region of the air-gap and EM regions. In addition, the magnetic fields from the PMs for Case C go to the stator through the shortest path since the permeability of the iron shell is large so that the magnetic flux tends to go into the shell perpendicularly. This indicates that the leakage flux in the iron stator is much less than the non-magnetic conducting stator or even the iron rotor.

Figure 10 shows that torque acting on the EM for each case. The results of torque computation are consistent with the behavior of the magnetic field as expected. Table 4 shows the maximum increasing torque % of each design compared to Case A. Based on the results, the EM with the same electrical current can generate 10% larger torque with the same structure but the different materials.

Table 3 DMP parameters of PM and image PM

$m_j (j=0,1) (\times 10^5)$	PM	Rotor	Stator
m_o	-2.29	3.16	4.20
m_l	6.18	-8.55	-11.30

where $n=6$ and $k=1$

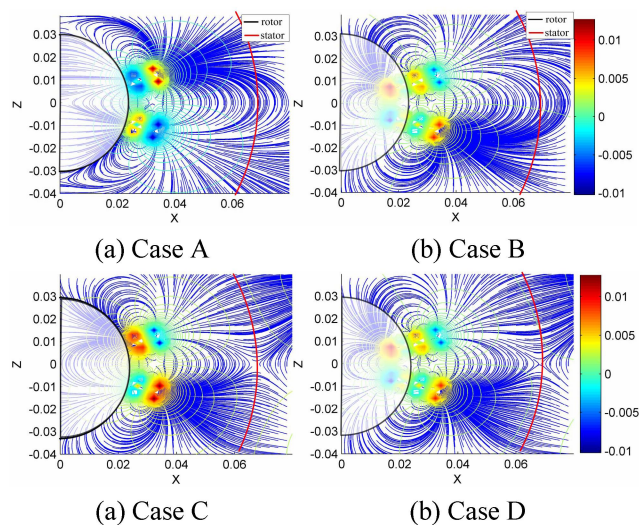


Fig. 9 Effect of the iron boundaries on magnetic field

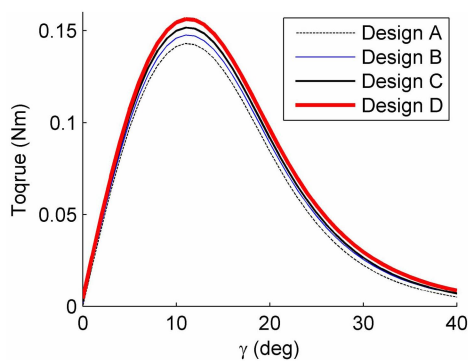


Fig. 10 Effect of the iron boundaries on torque of SWM

Table 4 Maximum torque (%)

Designs	B	C	D
Torque (%)	3.2	6.0	9.2

4. CONCLUSIONS

Image method with a DMP method which derives a relatively closed-form solution for computing boundary conditions in magnetic field has been presented. The methods, which extends the DMP method for calculating the magnetic field in free space, offers an effective means to account for the certain solution forms for some important problems involving straight-line, circular and spherical boundaries.

With the simplicity but accuracy of the method, the method can be used not only for the design of the material of an electromagnetic actuator but also the accurate computation of the force/torque. Two illustrative examples have demonstrated the effectiveness and simplicity of the modeling method. Specially, the method offers an inexpensive means to reduce the computational effort for calculating the magnetic force/torque and visualize the field interaction between the magnetic field by PMs and boundaries. These advantages will make the method an attractive alternative to the existing methods such as numerical FE method. We expect that the DMP method with the image method presented here provides a basis for other magnetic field analyses for example, effects of iron core electromagnet, modeling of an eddy current in a magnetic conducting material, etc.

REFERENCES

- [1] B. Shchokin and F. Janabi-Sharifi, "Design and kinematic analysis of a rotary positioner," *Robotica*, vol. 25, pp. 75-85, 2007.
- [2] M. T. S. Kokaji, N. Mishima, H. Maekawa, and T. T. a. K. A. K. Kaneko. vol. 2007.
- [3] K.-M. Lee, Q. Li, and H. Son, "Effects of numerical formulation on magnetic field computation using meshless methods," *IEEE Transactions on Magnetics*, vol. 42, pp. 2164-2171, 2006.
- [4] H. Ghoizad, M. Mirsalim, M. Mirzayee, and W. Cheng, "Coupled magnetic equivalent circuits and the analytical solution in the air-gap of squirrel cage induction machines," *International Journal of Applied Electromagnetics and Mechanics*, vol. 25, pp. 749-754, 2007.
- [5] K.-M. Lee and H. Son, "Distributed multipole model for design of permanent-magnet-based actuators," *IEEE Transactions on Magnetics*, vol. 43, pp. 3904-3913, 2007.
- [6] Y. Saito, K. Takashi, and S. Hayano, "Finite element solution of unbounded magnetic field problem containing ferromagnetic materials," Vancouver, BC, USA, 1988, pp. 2946-8.
- [7] G. Xiong and S. A. Nasar, "Analysis of fields and forces in a permanent magnet linear synchronous machine based on the concept of magnetic charge," *IEEE Transactions on Magnetics*, vol. 25, pp. 2713-2719, 1989.
- [8] L. Kapjin and P. Kyihwan, "Modeling eddy currents with boundary conditions by using Coulomb's law and the method of images," *IEEE Transactions on Magnetics*, vol. 38, pp. 1333-40, 2002.